Pattern of vertical velocity in the Lofoten vortex (the Norwegian Sea)

Igor Bashmachnikov[1,2], Tatyana Belonenko[1], Pavel Kuibin[3], Denis Volkov[4,5], Victor Foux[1]

[1] *Saint Petersburg State University,*
7-9, Universitetskaya nab., Saint Petersburg, 199034, Russia

[2] *NIERSC- Nansen International Environmental and Remote Sensing Centre,*
office 49H, 7, 14-th Line V.O., Saint Petersburg, 199034, Russia
ORCID: 0000-0002-1257-4197

[3] *Kutateladze Institute of Thermophysics, SB RAS,*
1 Lavrentyev Ave., Novosibirsk, 630090, Russia

[4] *Cooperative Institute for Marine and Atmospheric Studies,*
University of Miami, Miami FL, USA;

[5] *NOAA Atlantic Oceanographic and Meteorological Laboratory,*
Miami FL, USA;

E-mails: igorb1969@mail.ru, t.v.belonenko@spbu.ru,
kuibin@itp.nsc.ru, dlvolkov@gmail.com, victoryf1285@yandex.ru

Mean radial distributions of various dynamic characteristics of the permanently existing anticyclonic Lofoten vortex (LV) in the Norwegian Sea are obtained from an eddy permitting regional hydrodynamic MIT general circulation model. It is shown that the model adequately reproduces the observed 3D thermohaline and dynamic structure of the vortex. The obtained radial distribution of the mean vertical velocity is found to form a complex structure: with the upward fluxes along the axis in and above the anticyclonically rotating LV core, compensated by the downward fluxes in the vortex skirt. These vertical motions maintain the vortex potential energy anomaly against dissipation. This secondary circulation is generated by the centrifugal force and, to a lesser extent, by the horizontal dispersion of the vortex energy, both intensified towards the seasurface. Below the vortex core, the maximum downward vertical velocity converges towards the vortex axis with depth. At these depths, the secondary circulation is forced by Ekman divergence in the bottom mixed layer. The theory of columnar vortices with helical structure, applied to the LV, relate the radial profiles of the vertical velocity with those of the horizontal circulation. The theoretically predicted the radial patterns of the mean vertical velocity in the LV were close to those, obtained from the primitive equation ocean model, if approximating the radial patterns of the azimuthal velocity with the Rayleigh profile.

Key words: Norwegian Sea, Lofoten vortex, vertical velocity, divergence, MIT hydrodynamic model, columnar vortex

1. Introduction

An interest of the scientific community to mesoscale vortices of the ocean has been increased during recent decades, as the development of remote sensing technologies and of eddy-permitting numerical models permitted massive statistical analysis of their properties in the World Ocean (Volkov et al. 2008, Zhmur 2011, Chelton et al 2007; Chelton et al 2011). The results of the research have shown that vortices regionally play a significant role in formation of the large-scale distribution of thermohaline properties of ocean waters, exchange of matter

through frontal interfaces and affect the large-scale ocean dynamics (Maze et al 1997, Luo and Lu 2000, Golivets and Koshlyakov 2003, Wunsch and Ferrari 2004, Lozier 2010, Bashmachnikov et al 2015).

Mesoscale vortices, also anticyclonic subsurface lenses, are an important source for increasing biological productivity in many areas of the World ocean (McGillicuddy et al 2007; Hansen et al 2010). The increase can be due to a horizontal transfer of nutrients, or of the modification of the depth of the seasonal pycnocline, or of intensified vertical fluxes through the pycnocline in vortex cores (Vaillancourt 2003, Klein and Lapeyre 2009, McGillicuddy et al 2007; Hansen et al 2010; Gaube et al 2013).

Usually mesoscale eddies exist for a relatively short time, - a few months (Chelton et al 2007, Chelton et al 2011, Bashmachnikov et al 2015). For example, using satellite altimetry, Chelton et al (2007) obtained an exponential decrease of the number of eddies as a function of their lifetime. Less than 1% of the detected eddies survived for 2 months or more. Long-living eddies travel hundreds and thousands of kilometers through a variable oceanic background which adds uncertainty in studies of their mean properties and dynamics.

The mesoscale Lofoten vortex (LV), quasi-permanently existing in the central part of the Lofoten depression in the Norwegian Sea (68°-72° N and 2° W-10° E), is a rare natural phenomenon. It was first detected during repeated hydrographic cruises of 1970s and 1980s (Alekseev et al 1991, Romantcev 1991, Ivanov and Korablev 1995a,b, Pereskokov 1999), while latter satellite altimetry observations confirmed that the LV forms a nearly permanent signal (Fig. 1a), the sea-level anomaly of, on average, 15 cm, in the central part of the Lofoten Basin (Kohl 2007, Volkov et al 2013, Belonenko 2014). The anticyclonic rotation of the LV is detected from the sea-surface to the ocean bottom at about 3000 m depth (Bashmachnikov et al 2017b). However, the LV is not rigidly attached to a distinct feature of bottom topography, as it is usually the case for quasi-permanent mesoscale vortices in the open ocean (White et al 2007). Not directly interacting with the mean regional currents or steep topography, this anticyclonic vortex presents a "natural laboratory" for a study of decay and re-generation of mesoscale vortices in the ocean.

Even in the background of abnormally warm and salty Atlantic water reservoir of the Nordic Seas, the LV represents a lens with a positive temperature-salinity anomaly at the core depth levels between 300 and 1000 m and with the diameter of 80-100 km (Ivanov and Korablev 1995a, Volkov et al 2013, 2015, Bashmachnikov et al 2017b).

A number of recent studies has been exploring horizontal and vertical structure of the LV, as well as explaining the phenomenon of its high stability (Kohl 2007, Raj et al 2015, Volkov et al 2015, Bashmachnikov et al 2017b). In particular, field observations, as well as results of hydrodynamic simulations with Massachusetts Institute of Technology primitive equation general circulation model (MIT GCM), suggest that differential winter convection and the merger with other mesoscale anticyclons are the two main mechanisms for maintaining the LV against dissipative processes (Kohl 2007, Volkov et al 2015, Bashmachnikov et al 2017b). The mesoscale vortices in the basin, some of which eventually serve for re-generation of the LV, are mostly generated as a

result of the baroclinic instability of the Norwegian Current near the Lofoten Islands (Kohl 2007, Isachsen 2015).

In this paper, we focus on an almost unexplored subject of the spatial pattern of the vertical velocity in the LV. Being a consequence of non-geostrophic processes in ocean vortices and linked to the processes of their decay, these results will serve for better understanding of temporal evolution of mesoscale vortices in the ocean. The structure of this secondary circulation in the ocean vortices is typically difficult to derive from comparatively short time-series, as the relatively small vertical velocities associated with this circulation are masked by the stronger vertical motions generated by vortex dynamic instabilities or vortex (elliptic) deformations. In in-situ and model studies we typically observe such deformations, the most often characterized by two positive and two negative anomalies in relative vorticity and the associated upward and downward vertical velocities (Mahdinia et al 2016, Bashmachnikov et al 2017b, Pilo et al 2018). The vertical velocity patterns of the secondary circulation are mostly known for quasi-stationary vortices over seamounts (Mullineaux and Mills 1997, White et al 2007, Lavelle 2006). In this study, we take advantage of the 12-year long eddy-permitting regional MIT GCM simulations to explicitly derive the mean vertical velocity pattern for a subsurface anticyclonic forex not attached to a pronounced topographic bump. Further, we compare the velocity structure, obtained from the model, with that predicted by the theory for vortices with a helical structure of threads of relative vorticity (Kuibin and Okulov 1996, Alekseenko et al 1999).

2. Data

We used the same configuration of the MIT GCM as in Volkov et al (2015) or Bashmachnikov et al (2017b), the model results provided by Cooperative Institute for Marine and Atmospheric Studies University of Miami NOAA/AOML/PHOD. The horizontal resolution of the model is about 4x4 km in the Nordic Seas. The model has 50 geopotential vertical layers; the layer thicknesses vary from 10 m in the upper ocean to 456 m below 3000 m depth. The boundary conditions are taken from the global MIT-ECCO2 model (Estimating the Circulation and Climate of the Ocean, Phase 2)[1], and the initial conditions are based on World Ocean Atlas 2009. The both MIT models use Japanese Re-Analysis (JRA25) for atmospheric forcing. Tested against in-situ data, MIT GCM has been proved to fit well the observed structure and dynamics of the Atlantic Water in the Lofoten Basin (Nguyen et al 2011, Raj et al 2015, Volkov et al 2015).

The improved altimetry data-set AVISO14 (https://www.aviso.altimetry.fr/en/my-aviso.html) with the horizontal resolution 0.25°x0.25° (28x10 km in the Lofoten Basin), covering time period from 1993 to 2015 is used in this study. It has been shown that the new data-set, in particular, permitted to improve eddy detection capabilities: the number of detected eddies using AVISO14 increased as compared to the previous AVISO versions (Capet et al. 2014). When estimating current velocity and relative vorticity from the sea-level data, the noise was minimized by using the 7-point stencil width formulae (Arbic et al 2012). Applicability of the AVISO altimetry data-set for

[1] http://ecco2.jpl.nasa.gov

detection of the LV center and its excursions has been demonstrated by Soiland et al (2016), who combined AVISO data-set with an analysis of the trajectory of a RAFOS float, trapped in the LV during 9 months.

Further in this section we give an outline of the main features of the algorithm for derivation of the LV position, radii and trajectory using AVISO and MIT data-sets (see Bashmachnikov et al 2017 for details). For LV tracking, horizontal distributions of the relative vorticity at a fixed depth level are used. Initially (1st of January 1993), as the first guess, the center of a pronounced negative relative vorticity anomaly in the central part of the Lofoten Basin is selected as the LV center. Starting from the first guess, the position of the LV center within the patch of negative relative vorticity is refined using a set of relative vorticity profiles along several rays, originating in the center of the first-guess and covering a circle with the 30° increments. The "edge" of the selected patch of negative relative vorticity is then defined as the minimum distance from the LV center to a point along a ray where: either 1) the relative vorticity profile crosses zero, or 2) the relative vorticity profile forms a local maximum, or else 3) the rate of decrease of the relative vorticity slows down significantly (below 25% of its maximum rate along the initial segment of the ray). The latter two criteria helped detecting the LV boundary even when the LV core is connected by a bridge of negative relative vorticity with another anticyclone or a filament. Second, the LV center is recomputed as the "center of mass" of the obtained "edge" contour. Then the procedure is repeated for the refined center position. After three iterations, the final position of the LV center is obtained. The LV radius, under an assumption of the axisymmetric LV, is computed as the mean distance from the LV center to the "edge" contour. Additionally, the semi-major and the semi-minor axis of an ellipse, fitted to the "edge" contour, present the maximum and minimum radii, under an assumption of the elliptic LV. At the following field of relative vorticity, the same procedure is repeated, taking the previous position of the LV center as the first guess. Visual inspection showed that the algorithm is very robust and does not allow jumping to a neighboring anticyclonic structure, even when they are stronger than the LV surface signature. During 24 years of LV tracking (1236 time steps), only two artificial corrections of the LV positions in AVISO altimetry had to be done (one in 1994 and another one in 1996). Both algorithm failures occurred when the LV signal in altimetry became very weak and split between two closely connected anticyclonic structures. Visual inspection of these situations suggest that they may represent events of splitting of the LV into two vortices during the eddy interaction with two strong cyclones. When applying the algorithm to the MIT GCM results, no algorithm failures were detected.

For detection of the vertical thermohaline structure of the LV, in situ vertical temperature and salinity profiles from EN4 Hadley Center data base (https://www.metoffice.gov.uk/hadobs/en4/) were downloaded. The EN4 profiles pass more rigorous quality control procedures and better procedures for removal of duplicate profiles than in the alternative World Ocean Data-base 2013 (https://www.nodc.noaa.gov/OC5/indprod.html) (Good et al., 2013). The vertical profiles, that were within the distance of less than 0.75 times the LV radius from the LV center (detected from altimetry) were considered to represent the thermohaline properties of the LV core, while those at distances from 1.2-1.5 times LV radius were taken as the background profiles. To avoid using profiles in strong neighboring cyclones or anticyclones around the LV as the background, the profiles within absolute values of relative vorticity anomalies stronger that $2\ 10^{-5}\ s^{-1}$ around the LV were not considered. The difference of the thermohaline properties in and outside the LV core at the same depth levels was taken as the LV induced

anomalies. From 1236 weeks of the LV tracking, the LV thermohaline anomalies were obtained during 100 weeks. 90% of the results were obtained after 2008, during the period of a regular sampling of the Lofoten basin by Argo profiling floats (Fig. 1a).

3. Results

3.1. Thermohaline and dynamic structure of LV from in-situ data and model results

The high-resolution version of MIT GCM, used here, has been tested against observations in several previous studies (Kohl 2007, Volkov et al 2015, Belonenko et al 2017, Bashmachnikov et al 2017b). The results showed that the model is able to realistically reproduce water structure and dynamics of the Lofoten Basin, as well as of the LV itself. The main mechanisms responsible for the permanence of the LV in the basin (deep winter convection in the LV core and merger with other anticyclones) are also reproduced by the model. Here we extend the previous MIT validations, using satellite and in situ observations, to show that the model also reproduces the details of the 3D thermohaline and dynamic structure of the LV.

The results of our automatic tracking procedure (see Section 2) in MIT GCM and in AVISO altimetry data are consistent with the results by Kohl (2007) and by Raj et al (2015), respectively (Fig. 1b). The frequency of the LV center positioned in each of the grid cells of the study region provide similar results in MIT GCM and in AVISO data. In both data-sets the LV is typically found in a quite limited area of the Lofoten basin: 70% of time the LV center is found within the distance of the mean LV radius from its mean position, 90% of time – within the distance of 1.5-2 LV radii. Consistent with Kohl (2007), Volkov et al (2015) and Raj et al (2015), the data-sets show the dominating cyclonic propagation of the LV within the basin. However, the LV excursions are more confined to the center of the basin in MIT GCM than in AVISO.

For mesoscale eddies, the mean radial profiles of the azimuthal velocity and of the relative vorticity are often close to those of the Rayleigh vortex (Carton, 2001). For such vortex the ratio of the radial distance, at which core the azimuthal velocity reaches its maximum ( ), to the radial distance, where the relative vorticity ( ) changes sign, is: $r(\omega=0)/r(V_{\varphi,\max})=\sqrt{2}$ (Bashmachnikov et al 2017a). The LV dynamic radius (distance from the LV center, where relative vorticity crosses zero) in MIT GCM is 27±5 km (Fig. 1e), while the azimuthal velocity reaches maximum at 18-20 km from the vortex center. This is consistent with the Rayleigh radial profile of the azimuthal velocity. Perfectly consistent with MIT GCM results, in situ CTD, ADCP and glider surveys show the dynamic radius of 24-35 km, while the maximum velocity is reached at 17-20 km from the vortex center (Ivanov and Korablev 1995a, 1995b, Søiland and Rossby 2013, Søiland et al 2016, Yu et al 2017). In AVISO data-set, the LV dynamic radius is on average 50±10 km (Fig. 1e), nearly double of that in MIT GCM. Bigger LV radii in AVISO altimetry is a result of at least 6 times lower horizontal resolution of AVISO data-set, as compared to MIT GCM, as well as of a space-time smoothing during processing and gridding of the sea-level anomalies. However, correctly reproducing the LV size, MIT GCM underestimates the maximum azimuthal velocity of the LV, giving 30-50 cm s^{-1} in MIT GCM versus 50-80 cm s^{-1} observed in situ (Søiland and Rossby 2013, Søiland et al 2016, Yu et al 2017). The peak relative vorticity of the LV core is also lower: from -0.2 to -0.3 10^{-4} s^{-1} in MIT GCM (Fig. 1f, see also Volkov et al 2015, Bashmachnikov et al 2017b) versus -0.8 10^{-4} s^{-1}

observed in situ (Søiland and Rossby 2013, Søiland et al 2016, Yu et al 2017) or in AVISO altimetry (Fig 1f). These model underestimates may be due to a limited model resolution. The effect of the MIT GCM resolution on the LV has been investigated by Volkov et al (2015). It has been found that the 4-km resolution reasonably well reproduces the amplitude and the size of the eddy kinetic energy anomaly, formed by the LV, when compared to satellite altimetry results. However, the model apparently smooths out some details of the radial structure of the dynamic characteristics in the LV at their peak values.

The in situ vertical profiles of the azimuthal velocity in the LV, derived from CTD observations (Ivanov and Korablev 1995a, 1995b), ADCP observations (Søiland et al 2016), as well as glider observations (Yu et al 2017), is very closely reproduced by MIT GCM. The simulated azimuthal velocity (and relative vorticity) in the LV slightly increases from the seasurface down to its maximum between 500 and 1000 m. Further down, at 1200-1500 m depths, the mean values of both characteristics rapidly falls to the 1/4-1/5 of their maxima at the eddy core level (Bashmachnikov et al 2017b).

MIT GCM also well reproduces the observed vertical structure of thermohaline anomalies in the LV (Fig. 1c-d, see also Volkov et al 2015, Bashmachnikv et al 2017). The anticyclonic vortex core manifests itself as a positive anomaly of temperature and salinity between 100-200 m and 800-1200 m depth, well consistent with observations by Alekseev et al (1991), Ivanov and Korablev (1995a, b), Søiland and Rossby (2013), Yu et al (2017).

Importantly, in situ data, as well as MIT GCM simulations, show that, on average, the LV forms a negative temperature and salinity anomaly from 200 m depth up, increasing towards the sea-surface (Fig. 1c-d). This means that the sea surface temperature (SST) in the center of the anticyclonic LV typically should be lower than along the LV periphery. As an example, Figure 2a presents two snapshots of horizontal structure of satellite SST from the Multi-Scale Ultra-High Resolution SST (MUR SST, https://mur.jpl.nasa.gov/) and surface currents from AVISO altimetry. Figure 2b presents the results of MIT GCM for the same date in October 2012. The snapshots show a close correspondence between the satellite derived structure of the horizontal velocity, the shape and the size of the LV, as well as of other vortices in the basin, and the results of MIT GCM simulations (when comparing figures, one should account for the 6-times lower resolution of the altimetry maps as compared to the MIT simulations). Here we stress that the model well reproduces the seasurface negative temperature anomaly over the center of the LV, relative the vortex periphery (see also Raj et al 2015).

Being practically stagnant and appearing in the time-averaged current velocity fields of the Lofoten basin (in the satellite altimetry, as well as in MIT GCM) as a compact mesoscale anticyclonic structure (Volkov et al 2015, Raj et al 2015, Bashmachnikov 2017c), the LV core also appears in climatology as a compact positive thermohaline anomaly. The time-averaged vertical profiles of temperature and salinity anomalies of the LV core, compared to the surrounding waters of the Lofoten Basin, obtained from the World Ocean Atlas 2013 (https://www.nodc.noaa.gov/OC5/woa13/) and from MIT GCM simulations, reproduce positive temperature and salinity anomalies at 300-1200 m depth and negative temperature-salinity anomalies above (Fig. 2c, compare to Fig. 1c-d). Somewhat lower mean temperature and salinity anomalies in the climatology should be attributed to a

stronger blurring of the LV vertical structure from sparse and episodic in-situ observations (compare with Fig. 1c-d).

The negative sea-surface temperature anomalies over the anticyclonic LV is not surprising. They are often observed over subsurface anticyclones (Bashmachnikov et al 2013a, Ciani et al., 2017, Barcelo-Llull et al 2017). The anomalies can be formed by doming of isopycnals over the eddy core (Mullineaux and Mills, 1997; White et al., 2007), being a sign of the vortex secondary circulation, as well as by a differential advection of the surrounding water, trapped by an eddy (Bashmachnikov et al., 2013). The high similarity in the vertical and in the horizontal thermohaline and dynamic patterns of the LV in in-situ/satellite data and in the MIT GCM simulations let us assume that the model adequately reproduces patterns of the vertical velocity in the vortex.

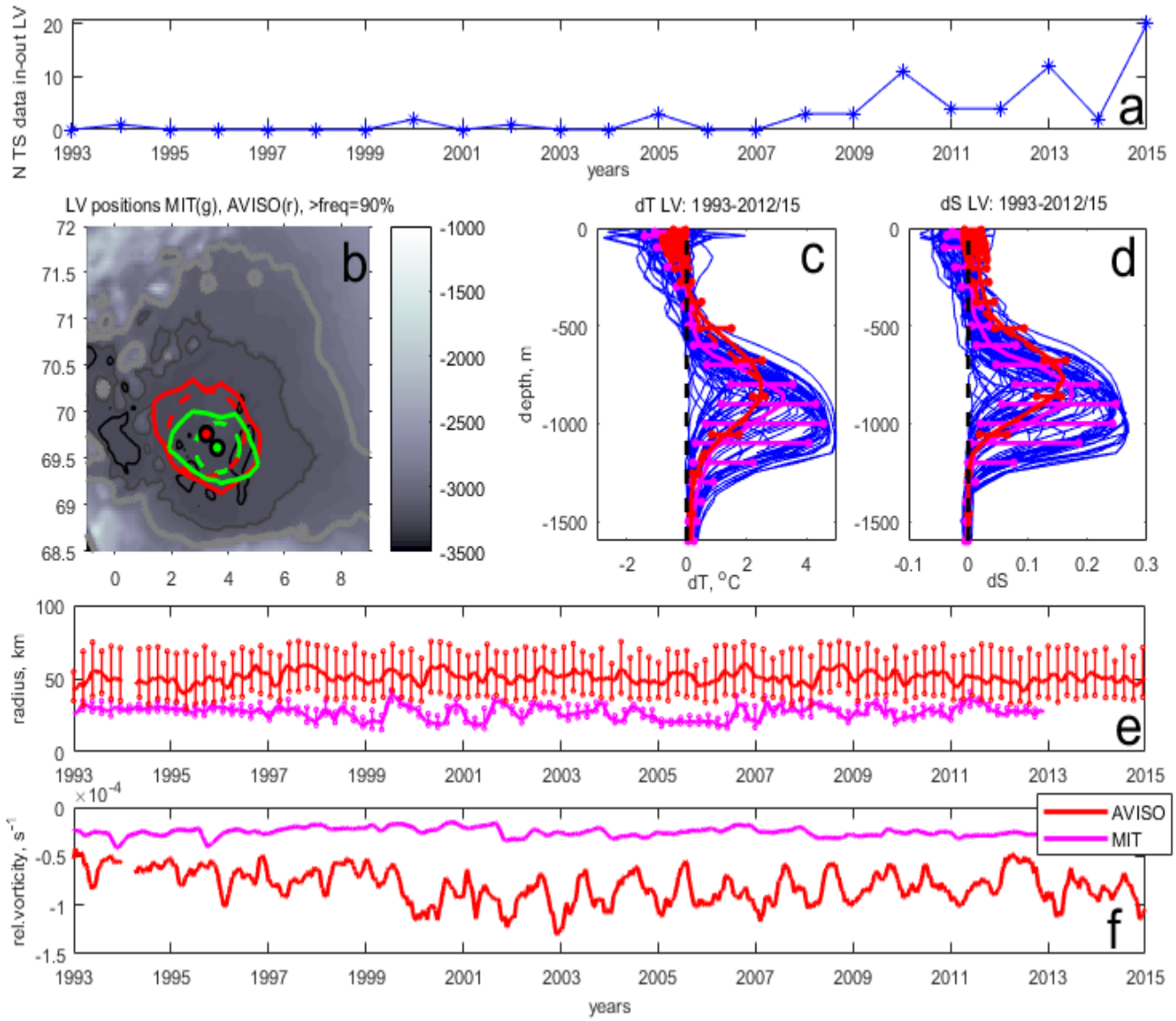

Fig. 1. Parameters of the LV from MIT GCM and observations. (a) Number of cases per year, when vertical profiles of temperature-salinity anomalies were constructed, using EN4 data base (see the profiles in panels (c) and (d)). (b) Mean positions of the LV center (dot), mean LV radius (dashed line) and the isoline limiting the area with 90% of observations of the LV center (solid lines) from MIT GCM (green) and AVISO altimetry (red).

Color presents bottom topography (m), isobaths of 2000 m (thick light gray line), 3000 m (thing dark gray line) and 3250 m (solid black line) are marked. (c) and (d) present vertical profiles of the temperature anomalies (c) and salinity anomalies (d) in the LV compared to the background from EN4 (blue lines). Mean profiles of in situ derived anomalies ± STD (magenta) and MIT GCM derived anomalies± STD (red). (e) time evolution of the LV radius (km) ± STD from AVISO (red) and MIT GCM (magenta). (f) time evolution of the LV peak relative vorticity (s^{-1}) from AVISO (red) and MIT GCM (magenta).

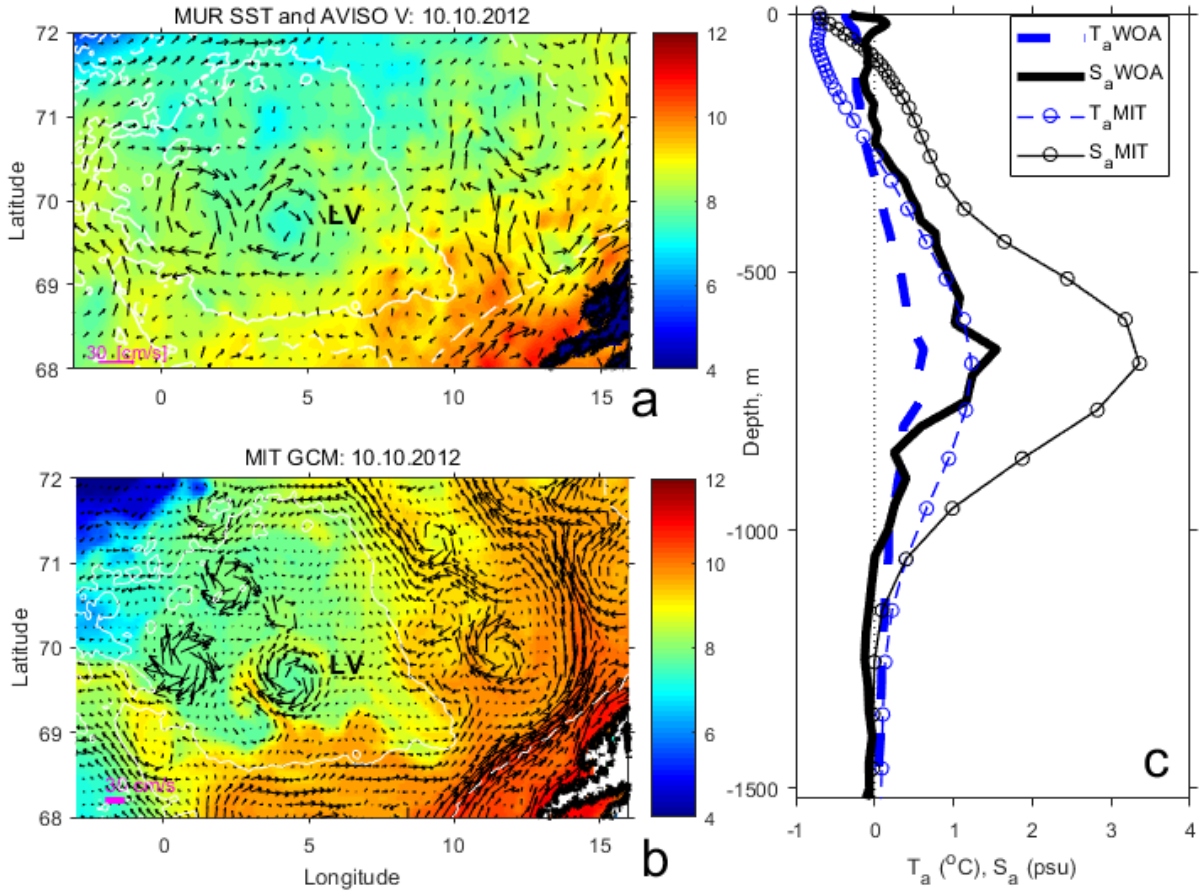

Fig. 2. (a) Sea-surface temperature from MUR data-set (colour, °C) and AVISO satellite altimetry currents (vectors) in the Lofoten basin for 10.10.2012. (b) The sea-surface temperature (colour, °C) and current velocity (vectors, only every 3rd vector is presented) in the Lofoten basin from MIT GCM for 10.10.2012. (c) Vertical profiles of the mean temperature anomalies (dashed blue lines) and salinity anomalies (solid black lines) inside the LV relative to the surrounding ocean: from the World Ocean Atlas 2013 (fat lines) and MIT GCM (thin lines with circles) averaged from 1993 to 2012. For visibility the scale for salinity anomalies is increased 50 times (the maximum salinity anomaly in the LV, derived from MIT GCM is 0.07).

The MIT GCM derived snapshot distributions of the relative vorticity and of the vertical velocity in the LV (Fig. 3) show intensive dynamic perturbations along the LV boundary of the second azimuthal mode (2 maxima and 2 minima). The perturbations are propagating along the LV boundary at about 1/3 of the maximum LV azimuthal velocity, consistent with the propagation of the second azimuthal mode, generated by baroclinic instability of the vortex (Paldor, 1999). The dominance of the first azimuthal instability mode in the LV has been discussed by Bashmachnikov et al (2017b) and is consistent with very high-resolution simulations of ocean vortices with similar Rossby and Burger numbers (Mahdinia et al 2016). When removing the background field of relative

vorticity, related to the nearly axisymmetric LV, higher and smaller positive relative vorticity anomalies just outside the LV radii (left panels of Figure 3) become positive and negative anomalies. Such anomalies are typical for wave-like dynamic instability patterns in a vortex (Mahdinia et al 2016). The maxima and minima of vertical velocity (right panels of Figure 3) fall in-between the relative vorticity maxima and minima, which typical for a progressive wave pattern. Therefore, besides consistency of the mean characteristics of the LV in MIT GCM, we also state consistency of the vertical velocity patterns in dynamic perturbations at the LV boundary. This gives evidence that MIT GCM adequately reproduces vertical velocity patterns at scales of the LV and even smaller scales of its dynamic perturbations.

Figure 3 also shows that the mean field of vertical velocity of the vortex is largely hidden in much stronger dynamic structures of the vortex perturbations of smaller scale. This makes it difficult to derive the mean fields of vertical velocity even in realistic model studies of ocean eddies. However, the LV presents a rare example of a permanently existing mesoscale vortex structure, making this goal achievable.

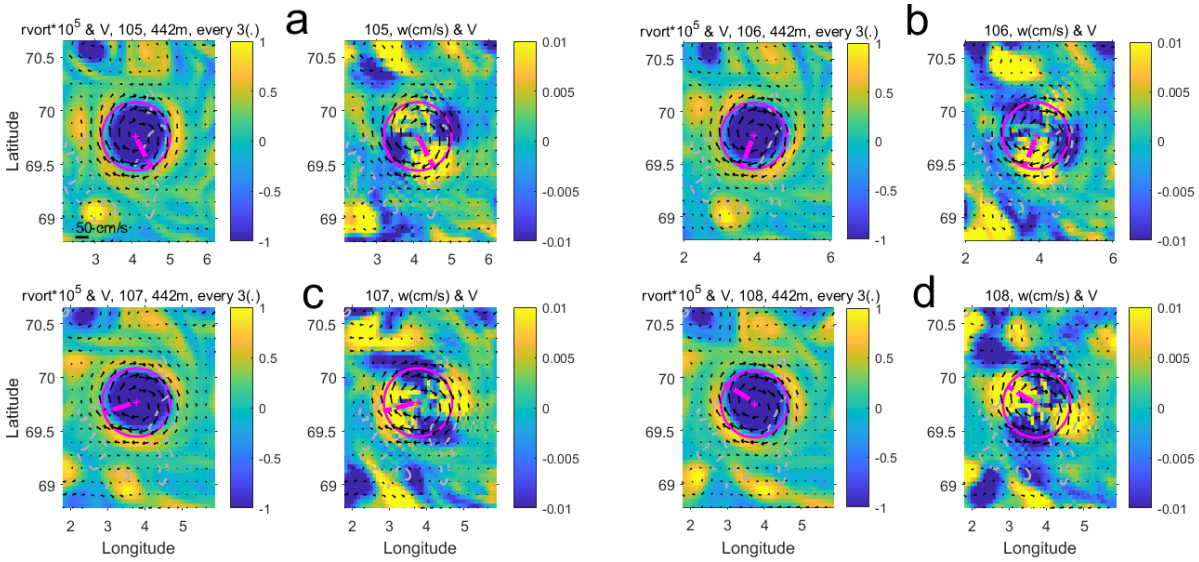

Fig. 3 A typical pattern of relative vorticity (x10^{-5} s^{-1}, left panels) and vertical velocity (m s^{-1}, right panels) in MIT GCM at 450 m depth for four consecutive time steps ((a) to (d)) with the time interval between the panel sets of 3 days. Magenta stars and circles mark the LV center and radius, respectively. The magenta dashed segment (starting at the LV center) mark from one panel to another the rotation of a maximum of vertical velocity of perturbations at the LV boundary.

3.2 Radial structure of dynamic parameters in the Lofoten vortex

To separate the mean patterns of the vertical velocity in the LV from the perturbations, in further analysis we consider the cylinder coordinate system bound to the LV center and the LV dynamic parameters averaged over the azimuthal coordinate and over the period of simulations. Figure 4 presents such *r-z* distributions of various dynamic characteristics of LV derived from the MIT GCM simulations. The maximum azimuthal velocity ($V_{\varphi,\max}$) at 20-23 km from the LV center (see black isolines in Fig. 4) and distance at which the relative vorticity

(ω) changes its sign, at 30 km from the LV center, are shown in the panels. The latter distance, $r(\omega=0)$, further in this paper is taken as the characteristic horizontal scale of the vortex (ε).

The time-averaged *r*-*z* distribution of the vertical velocity has a complex structure (Fig. 4a), indicating the presence of a divergence for both, the upper and the lower parts of the vortex. This has not previously been demonstrated neither in in situ, nor in model studies of mesoscale ocean vortices. The upward vertical velocity in the central part of the LV core and above explains the observed negative temperature (salinity) anomalies above the LV core (as observed in Figs. 1-2). At fixed depth levels, the radially integrated upward flux in the central LV core, is roughly compensated by the radially integrated downward flux at the LV skirt at all depth levels from 0 to 1000 m. The latter is integrated in the range of 12 - 30 km from the LV center (e.g. between red and magenta lines in Fig. 4a). This asserts consistency of the obtained mean radial structure of the vertical velocity.

In the LV skirt, at the lower part of the LV core (1200-1300 m), the downward flux is already about 20% stronger then the upward flux at the same levels, which assures the overall downward flux below 1300m. Below 1500-2000 m only downward vertical velocities are detected.

The maximum upward vertical velocity in the center of the LV core (the mid- and the upper ocean) is estimated to be V_0 ~2 × 10^{-3} cm s^{-1}, while the maximum downward vertical velocity at 2500 m (deep ocean) is more than 3 times less: $V_0 \approx$ -0.6 10^{-3} cm s^{-1} (Fig. 4a).

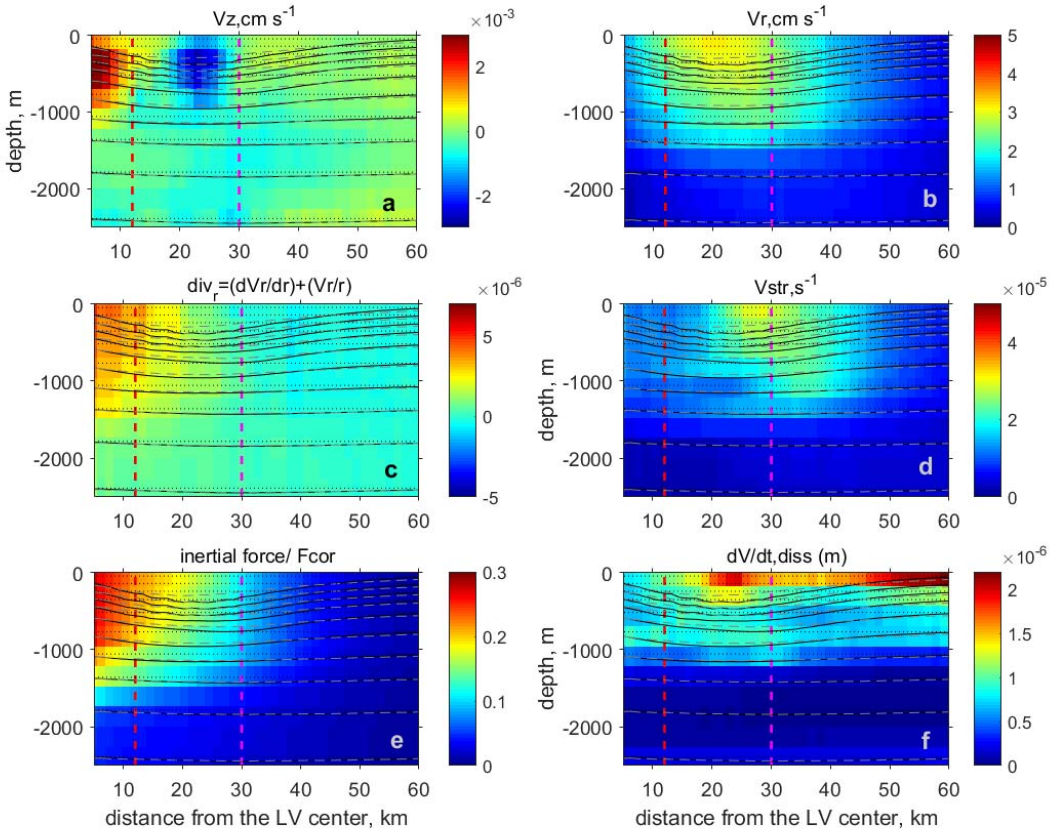

Fig. 4. Radial distribution of time-averaged characteristics in LV in MIT GCM results, averaged over 2 years of the model run: (a) vertical velocity (positive - upward, cm s^{-1}), (b) radial velocity (positive - outwards, cm s^{-1}), (c) radial divergence (positive –outwards, s^{-1}, see Eq,1), (d) horizontal shear stresses (s^{-1}), (e) ratio of the centrifugal force to the Coriolis force, (f) variation of horizontal velocity due to energy dissipation (m). The radial distributions of the azimuthal velocity (black solid lines) and radial velocity (gray dashed lines) for different vertical levels (out of scale) are given with a vertical offset to become zero at the corresponding depth level (see the dotted horizontal zero-velocity lines). Red and magenta vertical dashed lines mark distances of 12 km (depth-mean vertical velocity at the LV core crosses 0) and of 30 km (depth-mean relative vorticity at the LV core crosses 0), respectively.

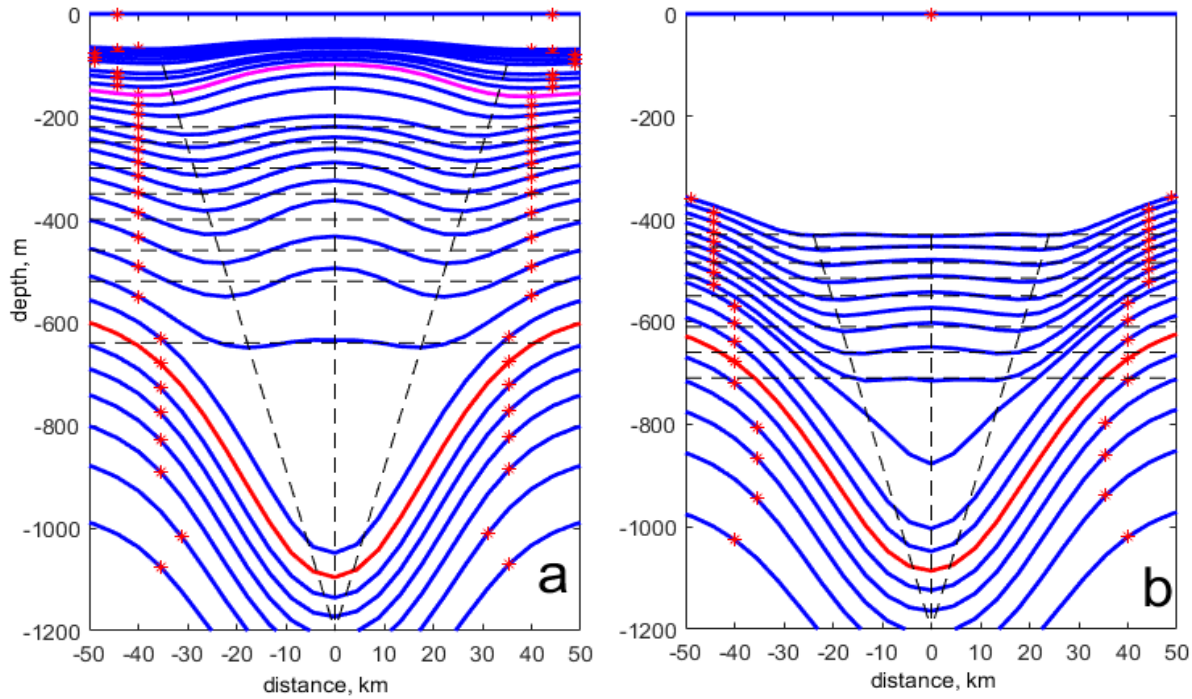

Fig. 5. Mean isopycnal depths (blue lines) across the LV for the two typical configurations of isopycnals in the LV: (a) for warm season, (b) for cold season (when deep convection in the LV core was detected). Red stars mark the LV points, where relative vorticity changes sign, magenta and red isopycnals mark the upper and the lower boundaries of the LV core, respectively. Horizontal dashed lines mark selected depth levels; vertical and tilted dashed lines mark local LV maximum and minima in the isopycnals depths inside the LV core.

The robustness of the mean vertical velocity pattern is confirmed by vertical sections of the mean isopycnal structure, derived from the MIT GCM simulations (Fig. 5). Averaged over the warm period (83% of the model time, Fig. 5a), as well as over the cold period, when deep convection reached the LV core, (17% of the model time, Fig. 5b), the isopycnals are shallowing in the eddy center and deepening along the eddy periphery at least down to 600-700 m depth. (see Bashmachnikov et al 2017b for classification of the patterns). This perfectly corresponds to the distance at which upward and downward vertical velocities are observed (Fig. 4a). The isopycnals bend-down converges towards the LV center with depth to form the shape of the overall downward looking isopycnals in the LV center below 800 m. This is consistent with the convergence of the downward vertical flux in Figure 4a. Figure 5b demonstrates that the vertical velocity pattern in the LV largely remains unchanged even during the episodes of deep convection in the upper part of the LV core (Fig. 5b): the maxima and the minima in the depths of isopycnals remain at the same distance from the LV center as they were during the warm season (Fig. 5a), although their amplitudes decrease. This suggests overall weaker vertical circulation in the LV during the episodes for deep convection.

By continuity, the vertical motions in an axisymmetric vortex are associated with radial convergence and divergence. The continuity equation for an axisymmetric ($\frac{\partial V_\varphi}{\partial \varphi} = 0$) vortex in cylinder coordinates is written as:

$$\left[\frac{V_r}{r}+\frac{\partial V_r}{\partial r}\right]+\frac{\partial V_z}{\partial z}=0, \quad (1)$$

The model derived radial divergence, the term in square brackets of Eq. (1), is presented in Fig. 4(c). In the upper 1700 m layer the radial divergence clearly intensifies towards the LV center and towards the sea-surface. It decreases to zero in the vortex skirt (at $r\sim r(\omega=0)$) and below 1700-m level. The derived pattern is consistent with that of the vertical velocity (Fig. 4a).

The radial and the vertical velocities in the vortex are linked to ageostrophic effects. In the LV the simulated radial flow velocities (Fig 4a) are an order of magnitude smaller than the azimuthal ones (Fig. 4b). In MIT GCM, the LV Rossby number is ~0.1 (Bashmachnikov et al 2017b), and this ratio corresponds to the ratio of the ageostrophic to the geostrophic velocity components in mesoscale eddies with such a small Rossby number (Carton 2001, Barcelo-Llull et al 2017).

The ageostrophic effects in eddies are related to the effect of the centrifugal force and friction. The radial velocities reach maximum in the region, where the azimuthal velocities are at maximum (Fig. 4b). Therefore, the radial velocities may result from the inertial effects. The ratio of inertial (centrifugal) to the Coriolis force (Fig. 4e), $\left[\frac{V_\varphi^2}{r}\right]\Big/\left[f\ V_\varphi\right]$, in the LV core is 0.2-0.3, typical for mesoscale vortices with low *Ro* (Carton 2001), and close to the ratio of the radial to azimuthal velocities.

The maximum radial velocities (Fig. 4b) are confined to the inner boundary of the region of maximum shear stress (Fig. 4d), where the processes of the turbulent exchange across the boundary of the vortex are the most intensive. The horizontal velocity decay rate due to turbulent dissipation is one of the standard MIT GCM outputs (Adcroft et al 2018). In the upper core the decay rate reaches maximum in the inner LV skirt (Fig. 4f), in-between the region of the maximum velocity and the maximum strain. The horizonal velocity dissipation rate strongly increases towards the sea-surface. Along the LV axis the strongest maximum of the decay rate underlies the LV faster rotating core at 800-1000 m depth. The very similar structure is obtained for the velocity dissipate rate from in situ microstructure measurements (Fer et al 2017). However, the dissipation rates in the model are smaller than the observed ones. Intensified towards the sea-surface, both the inertial forces and the turbulent diffusion of momentum induce intensification of the radial divergence towards the sea-surface and upward vertical velocities in the upper part of the LV core. The ratio of the velocity variations due to turbulent dissipation to Coriolis force is around 0.02-0.04, an order of magnitude smaller than the effect of the inertial force (Fig. 4e). Thus, we can assume that the radial ageostrophic component of the current velocity is primarily associated with centrifugal forces, not with the vortex decay through the turbulent diffusion of momentum across the vortex skirt. Figure 3 presents traces of filaments at some distance outside the LV dynamic radius, especially well seen behind positive and negative anomalies of vertical velocity.

Besides the abovementioned forces, the divergence in the LV core is, sometimes, associated with a local divergence of the Ekman fluxes, caused by the perturbation of the wind field by the vortex (Gaube et al 2013). The resulting vertical velocity is estimated as (Gaube et al 2013):

$$V_{0E} = -\frac{3C_d \rho_a |V_a|}{2\rho f} \overline{\omega}_z ,$$

here C_d is wind friction coefficient, ρ_a=1.2 kg m^{-3} is air density, ρ=1030 kg m^{-3} is density of water, f=1.4 10^{-4} c^{-1} is Coriolis parameter, V_a is wind speed in the driving layer, $\overline{\omega}_z$ – mean relative vorticity of the vortex core. Taking ρ_a / ρ=10^{-3}, C_d=10^{-3} (Bowden 1983) and V_a=5 m s^{-1} and $\overline{\omega}_z$=3 10^{-5} c^{-1} in the upper part of the LV core, we get the corresponding vertical velocity: V_{0E} = 1.5 10^{-4} cm s^{-1}. V_{0E} is an order of magnitude smaller than observed in the center of the LV (Fig. 4a). Therefore, the effect of local Ekman divergence due to eddy induced wind variations over the LV can be neglected.

The registered downward motion below the central parts of the LV core (1500 m and below, Fig. 4a) may be associated with Ekman divergence of the anticyclonic flow in the presence of bottom friction. The characteristic vertical velocity can be estimated as (Pedlosky 1987):

$$V_0 = C \overline{\omega}_z , \qquad (2)$$

where $C = \sqrt{\frac{K_z}{2f}}$, K_z is coefficient of vertical turbulent viscosity and $\overline{\omega}_z$ is mean relative vorticity at the bottom. For $V_{\varphi,\max}$ ~ 10 cm s^{-1}, we define $K_z \sim 2.5 \cdot 10^{-3} V_\varphi$ ~ 2.5*10^{-4} m^2 s^{-1} (Bowden 1983), which is in the range of the values observed for the turbulent exchange in the bottom layer in the presence of mesoscale vortices (Bashmachnikov et al 2013b, Ozmidov 1986, Siedler et al 2001). Taking the average relative vorticity in the lower part of the LV from the MIT GCM results, $\overline{\omega}_z \approx$ -3 10^{-6} s^{-1}, we get $V_0 \approx$ -0.5 10^{-3} cm s^{-1}. V_0 is close to the vertical velocity registered at the bottommost levels of the model simulations (Fig. 4a). Thus, the bottom friction can cause the observed downward velocities in the lower part of the vortex.

3.3 Radial pattern of the vertical velocity from patterns of the eddy azimuthal velocity

An analysis of the experimental data of vortex dynamics suggests that the vorticity lines in the vortices are often not rectilinear but helical (Kuibin and Okulov 1996, Alekseenko et al 1999). If we assume, that the vorticity lines can be approximated by canonical helical spirals, the azimuthal (circumferential) and the axial (vertical) velocity components in an axisymmetric vortex can be linked given a radial distribution of the vertical component of relative vorticity (Kuibin and Okulov 1996). In this approach, the center of the radial distributions slides along the helical thread, along which the characteristics of the vortex do not change. Certainly being a simplification of the real vortices, this approach, however, allows us reducing the model dimensions from 3D to 2D. A detailed description of the theory of vortices with helical symmetry is given by Kuibin and Okulov (1996), Alekseenko et al (1999, 2007).

Intense geophysical vortices in the atmosphere, like tornado, are often observed to the form the helical spirals. This phenomenon is dynamically related to interaction of the vortices with other dynamic structures, which induce instabilities of the vortices (Alekseenko et al 2007). There are no direct observations of the helical structure of ocean vortices, which is due to technical difficulty for deriving detailed snapshot structure of ocean vortices. However, observations of intense atmospheric vortices, as well as tilting of the axis of oceanic vortices (Walsh et al 1997; Bashmachnikov et al 2013a) suggest the latter to hold a similar structure.

The application the theory of helical vortices to oceanic structures is given in Belonenko et al (2017), to which we refer reader for details. Here we limit our description to the most important outputs of the theory. We consider the radial, azimuthal and vertical components of the velocity vectors of the vortex (V_r, V_φ, V_z) and of the relative vorticity vector $(\omega_r, \omega_\varphi, \omega_z)$ in the system of the cylindrical coordinates (r, φ, z), centered at the vortex axis – the peak relative vorticity of the vortex core. In the following theoretical estimates we assume the radial velocity in the vortex core $V_r = 0$ everywhere, except for the upper and the lower boundary of the vortex. Thus, we assume the areas of the fluid divergence to be all above and below the vortex core (in the near-surface and in the near-bottom layers), limiting the obtained solutions to the intermediate depths of the subsurface core of the vortex. This is a certain simplification, as it follows from our previous discussion (Section 3.2 and Fig. 4b-c), but the observed intensified vortex divergence in the upper ocean and near the bottom justifies this approach. The two components of the velocity of an axisymmetric columnar vortex then can be written as (Kuibin and Okulov 1996):

$$V_\varphi = \frac{1}{r}\Phi(r), \tag{3}$$

$$V_z = V_0 - \frac{1}{l}\Phi(r),$$

here V_0 is the axial vertical velocity ($V_0 = V_z(r=0)$), $h = 2\pi l$ is the vertical spacing between the helical lines of relative vorticity.

As

$$\omega_z = \frac{1}{r}\frac{\partial}{\partial r}(rV_\varphi), \tag{4}$$

in view of equation (3), for an axisymmetric vortex, function $\Phi(r)$ can be determined through the radial distribution of the relative vorticity (ω_z):

$$\Phi(r) = \int_0^r \omega_z(r')r'dr', \tag{5}$$

When the flow is barotropic incompressible and non-viscous, the velocity field (4) satisfies the Euler's equations for any radial distribution relative vorticity. The continuity equation for the non-divergent ($V_r = 0$)

axisymmetric ($V_\varphi = 0$) vortex core region is written as: $\frac{\partial V_z}{\partial z} = 0$, and dependence of vertical velocity on the coordinate z can be neglected. This equation is satisfied, in particular, for (Eq. 3):

$$V_0(z) = const\ ,\ \frac{\Phi(z)}{l(z)} = const\ . \tag{6}$$

We apply Eq. (6), neglecting relatively small vertical variations of V_0 in the LV core region, at 100 -800 m depth (Fig. 4a). Further, consistent with observations (Section 3.2) and as it follows from the non-divergent character of the flow, for any depth level from the selected range, the integral of the vertical velocity over the area of the vortex is assumed to be zero:

$$Q = 2\pi \int_0^{n\varepsilon} r' V_z dr' = 0 \tag{7}$$

Here n (not necessarily an integer) is taken, so that the distance $n\,\varepsilon$ (ε is the vortex dynamic radius) marks the limit of the valid solution. Naturally, for any of theoretical continuous distributions of the relative vorticity assumed in Eq. (4), the value n must be chosen such that at $r \geq n\,\varepsilon$ all the dynamic characteristics of the vortex are significantly smaller then those in the vortex core. In particular, for the vertical velocity, the following should be true:

$$V_z(n\,\varepsilon)/V_0 << 1 \tag{8}$$

The solution of Eqs. (3-7) depends on a radial distribution of the relative vorticity (ω_z) in the vortex. In this paper we use three common radial distributions: Scully (1975), Rayleigh (Carton 2001, Bashmachnikov et al 2015) and Q (Batchelor 1964).

For Scully vortex $\omega_z = \frac{\Gamma}{\pi}\frac{\varepsilon^2}{\left(r^2+\varepsilon^2\right)^2}$, where Γ=const is the vortex circulation. Applying Eqs.(7-8), we select the smallest n, such that $V_z(n\,\varepsilon)$ less than 10% of $V_0(n)$ (Fig. 6a). This is satisfied for n=5.2, and the radial distribution of the vertical velocity is (Belonenko et al 2017):

$$V_z(r) = V_0\left(1 - \frac{r^2}{0.877\left(r^2+\varepsilon^2\right)}\right), \text{ where } V_0 = 0.4\frac{\Gamma}{\pi l} \text{ and } r \leq 5.2\varepsilon \tag{9}$$

For Q-vortex, also known as the Batchelor vortex (Batchelor 1964), $\omega(r_z) = \frac{2\alpha\Gamma}{\pi}\exp\left(-\alpha r^2\right)$. As in (Bashmachnikov et al 2017a), we take $\alpha = \frac{1}{0.5\varepsilon^2}$, so that the maximum azimuthal velocity of the Q-vortex is close to that of the Rayleigh vortex for the same ε. $V_z(n\,\varepsilon)$ less than 1% V_0 is reached already for $n \geq 2.3$ (Fig. 6a). However, for such n, an azimuthal velocity at this distance from the vortex center is still over 50% of its maximum value. Therefore, we take n = 4 as the breakpoint of the solution (Bashmachnikov et al 2017a):

$$V_z = 1.032 \cdot V_0\left[\exp\left(-2r^2/\varepsilon^2\right) - 0.031\right], \text{ where } V_0 = \frac{\Gamma}{\pi l} \text{ and } r \leq 4\varepsilon\ . \tag{10}$$

For Rayleigh vortex, $\omega_z(r) = \frac{\Gamma}{\pi\varepsilon^2}\left(1-\frac{r^2}{2\varepsilon^2}\right)\exp\left(-\frac{r^2}{2\varepsilon^2}\right)$, the $|V_z(n\varepsilon)/V_0|$ is below 1% is reached in a limited region with minimum at n = 1.9 (Fig. 6a). The resulting solution is (Belonenko et al 2017):

$$V_z(r) = V_0\left[1-\frac{r^2}{0.6\,\varepsilon^2}\exp\left(-\frac{r^2}{2\varepsilon^2}\right)\right], \text{ where } V_0 = 0.3\frac{\Gamma}{\pi l} \text{ and } r \le 1.9\varepsilon \quad (11)$$

The advantages and disadvantages of Scully, Rayleigh and Q – vortices in approximation of the time-averaged radial structure of different dynamic parameters of the LV are seen in Fig. 6(b-d). For of Q-distribution the radial characteristics decrease more rapidly with r, than for Scully-distribution, and better approximate the LV radial structure. Further, in Scully-vortex, with increasing n, V_0 amplifies to infinity, which is not the case for Q-vortex. Nevertheless, all the radial distributions of the presented dynamic characteristics of the LV are better approximated by Rayleigh distribution (Fig. 6b-d). Only Rayleigh distribution allows a region of positive relative vorticity and negative azimuthal velocity in the vortex skirt (Fig. 6b,d). However, the essential deficiency of using Rayleigh distribution, with the assumptions Eqs.(7-8), is that the criterion Eq.(8) is satisfied only in a very limited range of r-values (Fig. 6a), and we are forced to "cut off" the solution at a rather significant value of the vortex azimuthal velocity and the relative vorticity (Fig. 6c).

Since we did not consider the regions of horizontal divergence in the theoretical solution, there is no mean for estimating the maximum vertical velocity in the vortex center (V_0). However, Eqs. (9-11) permit to conclude, that the same dynamic radius and the same maximum azimuthal velocity, V_0 in Rayleigh distribution is 2.5-3 times higher than that for Scully or Q-distributions. The higher V_0 of Rayleigh distribution is a result of assumption Eq. (7) in presence of the downward motions at the periphery of the vortex core, not present in Scully or Q-distributions.

The theoretical approximations of the dynamic characteristics in the region of relatively homogeneous vertical structure of the vertical velocity below the LV core (Fig. 7), also show the advantages of the Rayleigh distribution as compared to other radial distributions used.

The results show stronger deviations of the mean velocity pattern from the Rayleigh distribution with distance from the LV center. A stronger cyclonic vorticity in MIT GCM simulations at distances over 50-60 km from the LV center versus the theoretical Rayleigh profile is due to an influence of two or three cyclonic vortices most of time surrounding the LV (Volkov et al., 2015). These vortices distort the inherent dynamic properties in the outer skirt of the LV (Figs. 6b-c, 7a-b), responsible for a stronger deviation of the radial profiles of vertical velocity from the theoretical ones (Figs. 6d, 7c). The presence of the cyclonic structures at the LV periphery may be a sign the LV energy decay via formation of ringlets (Nof 1993).

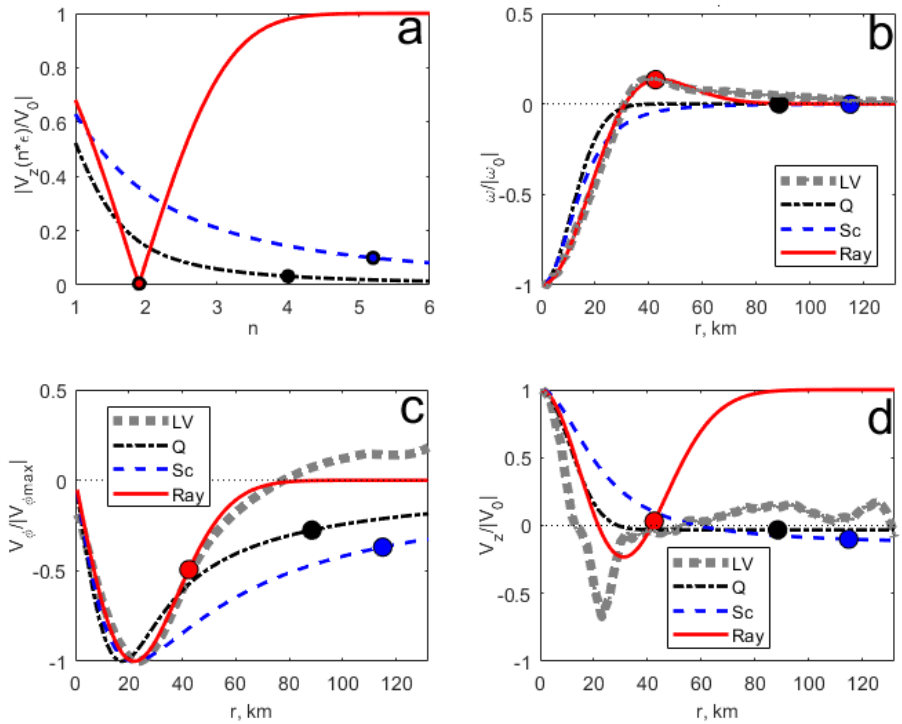

Fig. 6. Normalized dynamic characteristics of LV core, 0-1000 m (gray dotted curves), and the theoretical results with $\varepsilon = 22$ km for Scully vortex (blue dashed curves), Rayleigh vortex (red solid curves), Q-vortex (black dash-dotted curves): (a) the absolute value of the normalized vertical velocity $\left|V_z(n\varepsilon)/V_0(n)\right|$ as a function of n. The solution artificial cut off at $r = n\varepsilon$ is marked by filled circles. For Q-vortex n=4, for Scully vortex n=5.2, for Rayleigh vortex n=1.9; (b) radial pattern of the normalized relative vorticity; (c) radial pattern of the normalized azimuthal velocity and (d) radial pattern of the normalized vertical velocity. We consider the solutions only left of the corresponding cut-off points.

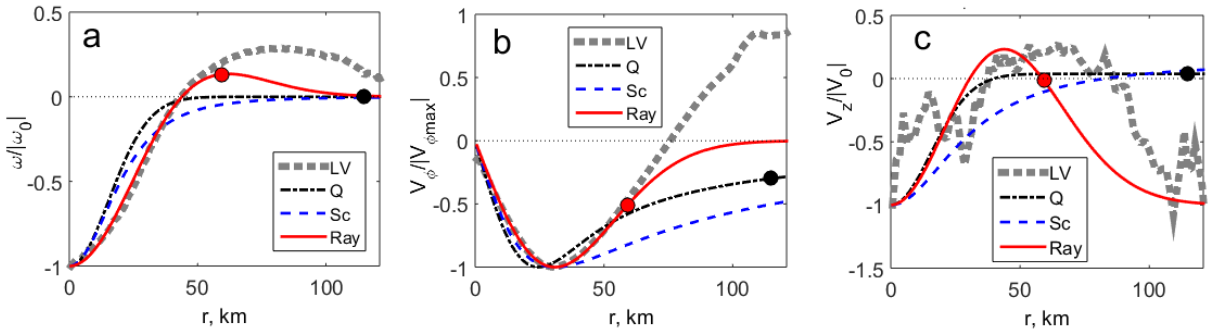

Fig. 7. Normalized dynamic characteristics of LV near the bottom, 1500-2500 m (gray dotted curves), and the theoretical results with $\varepsilon = 31$ km for Scully vortex (blue dashed curves), Rayleigh vortex (red solid curves), Q-vortex (black dash-dotted curves): radial changes of (a) normalized relative vorticity, (b) normalized azimuthal velocity and (c) normalized vertical velocity. Filled circles show the cut-off points for the selected n-values.

4. Discussion and Conclusions

In this paper we investigate 3D structure of thermohaline and dynamic parameters of the quasi-persistent subsurface Lofoten vortex in the primitive equation MIT GCM. Previous studies (Kohl 2007, Raj et al 2015, Volkov et al 2015, Isachsen 2015, Bashmachnikov et al 2017b) and our analysis show a close correspondence in the vertical and horizontal structure of the LV, compared to what is derived from in-situ and satellite observations. In particular, we showed that the model adequately reproduces 3D structure of thermohaline and isopycnic anomalies in the LV. We have also shown that the derived patterns of temperature, salinity and density anomalies in the vortex, as well as those of the radial velocity, are consistent with the model-derived time-average patterns of the vertical velocity. This confirms robustness of the mean vertical velocity field of the LV obtained from the MIT CGM simulations.

The results show, that when dynamic perturbations at the vortex boundary are removed, vertical velocity in the LV presents a rather complex pattern in $z-r$ space, schematically presented in Figure 8. This pattern reminds those of the secondary circulation in Taylor caps over the seamounts (Mullineaux and Mills 1997, White et al 2007), but has some important differences. The secondary circulation is found to be governed by the two regions with high horizontal divergence: above the core (also, a weaker one, at the core level) and near the bottom. Only the second one is reported for Taylor caps (Lavelle 2006, White et al 2007). Convergence of the maximum downward vertical velocity towards the vortex axis as water approaches the ocean bottom also is not observed in Taylor caps. Importantly, the upward vertical velocities in and above the core, coupled with the downward motions at the vortex periphery, increase the radial gradients of water density, thus maintaining the anticyclonic circulation against dissipation.

Fig. 8. Schematics of the vertical and radial velocity structure in an anticyclonic vortex with a subsurface core. The gray area is the vortex core, the gray arrow represents the main anticyclonic circulation of the vortex, black arrows represent the secondary circulation in the vortex.

The mechanisms for maintaining the secondary pattern are also not all the same as suggested for Taylor caps. As in Taylor caps, the lower part of the secondary circulation is forced by bottom friction in the bottom Ekman layer (Pedlosky 1987). However, in the LV, the near bottom divergence is fed by a weak convergence of the downward flows at the vortex core periphery above, and not by the ascending motions at the same depth levels (Mullineaux and Mills 1997). In the upper part of the LV, the divergence is found to be forced mostly by the centrifugal forces, while the turbulent decay of the azimuthal velocity is one order less (except in the uppermost ocean, where it may have a comparable effect). The importance of the inertial forces in ocean eddy dynamics has been previously highlighted (Carton 2001, Chelton et al 2011). In this paper we show a link between the inertial forces and the secondary circulation in the vortex. The wind forcing, suggested as one of the mechanisms forcing divergence in the upper parts of anticyclones (Gaube et al 2013), is also negligibly small for the LV, as the related vertical velocities were an order of magnitude less than those in the model.

In our study we also have shown that MIT GCM underestimates the peak azimuthal velocities in the LV, compared to in situ data (Soiland et al 2016, Fer et al 2017), therefore underestimates the relative role of the centrifugal forcing. The turbulent dissipation of horizontal velocity in the model is also underestimated, compared with observations (Fer et al 2017). This suggests a higher peak vertical velocity in the LV core in the real ocean.

Subsurface anticyclones are often characterized by negative SST anomalies over their cores (Bashmachnikov et al 2013a, Ciani et al 2015). It was previously suggested that the differential advection of the surrounding water into the core is the main reason for the observed negative SST anomalies over the anticyclonic Mediterranean water eddies (meddies) in the subtropical Atlantic (Bashmachnikov et al 2013a). The negative temperature anomalies in the LV are suggested to be associated with the secondary circulation over the LV core and the corresponding rise of the isotherms, since water temperature increases upward during all seasons (see, for example, Raj et al., 2015). The difference may be explained by difference in the core depths of the two types of eddies together with a the much lower f/N ration in the subtropics (see Bashmachnikov et al 2014, Ciani et al 2015, 2017). Having cores at 600- 1500 m, meddies do not directly influence the water structure in the strongly stratified subtropical upper ocean. The LV core is much shallower (200-1000 m), and the vortex induced near surface divergence and the associated rise of the isotherms results in overall negative SST anomalies over the vortex.

The radial structure of the vortex vertical velocity, derived from MIT GCM simulations, is further compared to the results of the theory of vortices with helical symmetry (Kuibin and Okulov 1996, Alekseenko et al 1999, 2007). The theory (Eqs. 3-5) permits relating radial profiles of vertical velocity to those of relative vorticity. Although the theoretical results use a strongly simplified vortex dynamic pattern by assuming divergence only

above and below of the core of an isolated vortex, the Rayleigh distribution presents a fairly realistic approximation of the radial vertical velocity pattern. In particular, the theoretical results demonstrate that, since in MIT GCM the peak relative vorticity in the LV core is underestimated, as well the simulations should underestimate the peak vertical velocity, as compared to observations. A weaker eddy rotation results in a weaker centrifugal force, and, consistently, in a weaker vertical velocity. Unfortunately, these conclusions are presently impossible to verify in the real ocean, as no observations of the vertical velocity in the LV are available.

Further theoretical advances are required, including account of the vortex divergence, to allow the theoretical evaluation of the peak vertical velocity along the vortex axis. Leaving the areas of horizontal divergence out of scope of the theoretical solutions, permits only defining radial profiles of the vertical velocity, but not to estimate the peak vertical velocity in the vortex corer ( ). Extending the theory to account centrifugal and/or decay of the vertical velocity due to turbulent dissipation will be an important step in estimating of the peak vertical velocities in ocean eddies from available observations of the horizontal velocity patterns.

Acknowledgments

The authors acknowledge support of Russian Science Foundation (RSF, project No. 18-17-00027). D. Volkov was supported by the NASA Physical Oceanography program (Grant NNX11AE27G) and by the base funds of NOAA Atlantic Oceanographic and Meteorological Laboratory.

References

Adcroft A, Campin JM, Dutkiewicz S, Evangelinos C, Ferreira D, Follows M, ..., Hill E (2018) MITgcm Documentation: 1-306.

Alekseenko SV, Kuibin PA, Okulov VL (2007) Theory of concentrated vortices. An introduction. Berlin, Heidelberg, New York, Springer, 506 p.

Alekseenko SV, Kuibin PA, Okulov VL, Shtork SI (1999) Helical vortices in swirl flow. J Fluid Mech 382:195–243.

Alekseev GV, Bagryantsev MV, Bogorodskiy PV, Vasin VV, Shirokov PE (1991) Structure and circulation of water in the area of anticyclonic eddy in the northeastern Norwegian Sea [in Russian]. Probl of the Arctic Antarct 65:14–23.

Barcelo-Llull B, Sangrà P, Pallàs-Sanz E, Barton ED, Estrada-Allis SN, Martínez-Marrero A, ... Marrero-Díaz Á (2017) Anatomy of a subtropical intrathermocline eddy. Deep Sea Res:I 124:126-139.

Bashmachnikov I, Boutov D, Dias J (2013a) Manifestation of two meddies in altimetry and sea-surface temperature. Ocean Sci 9(2):249-259.

Bashmachnikov I, Loureiro C, Martins A (2013b). Topographically induced circulation patterns and mixing over Condor seamount. Deep Sea Res II 98:38-51.

Bashmachnikov I, Carton X, Belonenko T (2014) Characteristics of surface signatures of Mediterranean water eddies, J Geophys Res, C119: 1-22, doi:10.1002/2014JC010244

Bashmachnikov I, Neves F, Calheiros T, Carton X (2015) Properties and pathways of Mediterranean water eddies in the Atlantic. Progr in Oceanogr 137:149-172.

Bashmachnikov IL, Belonenko TV, Kuibin PA (2017a) The application of the theory of the columnar Q-vortex with helical structure to the description of the dynamic characteristics of the Lofoten vortex of the Norwegian sea [in Russian]. Vestn St Petersburg Un-ta, Ser.7 62(3):221-336. https://doi.org/10.21638/11701/spbu07.2017.301.

Bashmachnikov IL, Sokolovskiy MA, Belonenko TV, Volkov DL, Isachsen PE, Carton X. (2017b) On the vertical structure and stability of the Lofoten vortex in the Norwegian Sea. Deep Sea Res:I 128:1–27. DOI: http://dx.doi.org/10.1016/j.dsr.2017.08.001.

Bashmachnikov IL (2017c) Seasonal and interannual variability of the position of the dynamic and thermal fronts of the Barents, Norwegian and Greenland seas [in Russian]. Materials of the conference "The Seas of Russia: science, security, resources", 3 - 7 October 2017: 29-30.

Batchelor GK (1964) Axial flow in trailing line vortices. J. Fluid Mech 20:645-658.

Belonenko TV, Bashmachnikov IL, Koldunov AV, Kuibin PA (2017) On the vertical component of velocity in the Lofoten vortex of the Norwegian Sea [in Russian]. Izvestiya, Atmospheric and Oceanic Physics 53(6):641–649. https://doi.org/10.1134/S0001433817060032

Belonenko TV, Volkov DL, Ozhigin VK, Norden YuE (2014) Circulation of waters in the Lofoten Basin of the Norwegian Sea, [in Russian]. Vestn S. Petersbur. Un-ta, Ser.7. 2:108-121.

Bowden KF (1983) Physical oceanography of coastal waters. Ellis Horwood Limited, Chichester, p. 302.

Carton X (2001) Hydrodynamical modelling of oceanic vortices. Surv Geophys 22:179-263.

Ciani D, Carton X, Bashmachnikov I, Chapron B, Perrot X (2015) Influence of deep vortices on the ocean surface, Discontinuity, Nonlinearity, and Complexity, 4(3), 281–311, doi:10.5890/DNC.2015.09.006

Ciani D, Carton X, Aguiar AB, Peliz A, Bashmachnikov I, Ienna F, Charron R, Santoleri R (2017) Surface signature of Mediterranean water eddies in a long-term high-resolution simulation. Deep Sea Research Part I: Oceanographic Research Papers, 130, 12-29.

Chelton DB, Schlax MG, Samelson RM, de Szoeke RA (2007) Global observations of large oceanic eddies. Geophys. Res. Lett. 34, L15606.doi:10.1029/2007GL030812

Chelton DB, Schlax MG, Samelson RM (2011) Global observations of nonlinear mesoscale eddies. Progr in Oceanogr 91:167-216.

Gaube P, Chelton DB, Strutton PG, Behrenfeld MJ (2013) Satellite observations of chlorophyll, phytoplankton biomass, and Ekman pumping in nonlinear mesoscale eddies. J Geophys Res C118. doi:10.1002/2013JC009027.

Fer I, Bosse A, Ferron B, Bouruet-Aubertot P (2018) The dissipation of kinetic energy in the Lofoten Basin Eddy. J Phys Oceanogr 48(6): 1299-1316.

Golivets SV, Koshlyakov MN (2003) Cyclonic vortices of the subantarctic front and formation of Antarctic intermediate water. Oceanology [in Russian] 43(3):325-338.

Hansen C, Kvaleberg E, Samuelsen A (2010) Anticyclonic eddies in the Norwegian Sea; their generation, evolution and impact on primary production. Deep Sea Res. I, 57(9), 1079-1091.

Isachsen PE (2015) Baroclinic instability and the mesoscale eddy field around the Lofoten Basin. J of Geophys Res 120 (4):2884-2903.

Ivanov VV, Korablev AA (1995a) Formation and regeneration of the pycnocline lens in the Norwegian Sea, [in Russian]. Russ Meteorol Hydrol 9:62–69.

Ivanov VV, Korablev AA (1995b) Dynamics of pycnocline lens in the Norwegian sea, [in Russian]. Russ Meteorol Hydrol 10:55-62.

Klein P, Lapeyre G (2009) The Oceanic Vertical Pump Induced by Mesoscale and Submesoscale Turbulence. Annual Review of Marine Science 1:351-375.

Kohl A (2007) Generation and Stability of a Quasi-Permanent Vortex in the Lofoten Basin. J Phys Oceanogr 37:2637-2651.

Kuibin PA, Okulov VL (1996) One-dimensional solutions a flow with a helical symmetry. Thermophysics and aeromechanics, 4:297-301.

Lavelle JW (2006) Flow, hydrography, turbulent mixing, and dissipation at Fieberling Guyot examined with a primitive equation model. J. Geophys. Res. 111:C07014. doi:10.1029/2005JC003224.

Lozier MS (2010) Destructing the conveyor belt. Science 328:1507-1511. doi:10.1126/science.1189250

Luo D, Lu Y (2000) The influence of negative viscosity on wind-driven, barotropic ocean circulation in a subtropical basin. Journal of Physical Oceanography 30(5):916-932.

Mahdinia M, Hassanzadeh P, Marcus PS, Jiang CH (2016) Stability of 3D Gaussian vortices in rotating stratified Boussinesq flows: Linear analysis. J. Fluid Mech., 824: 97-134, https://doi.org/10.1017/jfm.2017.303.

Maze JP, Arhan M, Mercier H (1997) Volume budjet of the eastern boundary layer off the Iberian Peninsula. Deep Sea Res:I 44:(9-10):1543-1574.

McGillicuddy DJ, Anderson LA., Bates NR, Bibby T, Buesseler KO, Carlson CA, ..., Hansell DA (2007) Eddy/wind interactions stimulate extraordinary mid-ocean plankton blooms. Science, 316(5827): 1021-1026.

Mullineaux LS, Mills S (1997) A test of the larval retention hypothesis in seamount-generated flows. Deep Sea Res 44:745-770.

Nguyen AT, Menemenlis D, Kwok R (2011) Arctic ice-ocean simulation with optimized model parameters: approach and assessment. J. Geophys. Res. 116: C04025. http://dx.doi.org/10.1029/2010JC006573.

Nof D (1993) Generation of ringlets. Tellus A 45(4):299-310.

Ozmidov RV (1986) Diffusion of an impurity in the ocean, [in Russian]. Leningrad, Gidrometeoizdat, 280 p.

Pedlosky J (1987) Geophysical fluid dynamics. Springer Verlag, 710 p.

Pereskokov AI (1999) On the physical nature of large-scale counter-cyclical cycle in the water column of the Norwegian Sea, [in Russian]. Reports of the Academy of Sciences 364(4):549-552.

Pilo GS, Oke PR, Coleman R, Rykova T, Ridgway K (2018). Patterns of vertical velocity induced by eddy distortion in an ocean model. Journal of Geophysical Research: Oceans, 123(3): 2274-2292.

Paldor N (1999). Linear instability of barotropic submesoscale coherent vortices observed in the ocean. J Phys Oceanogr, 29(7): 1442-1452.

Raj RP, Chafik L, Nilsen JEØ, Eldevik T, Halo I (2015) The Lofoten Vortex of the Nordic Seas. Deep-Sea Res:I I96:1–14.

Romantcev VA (1991) Large-scale structure and characteristics of the average circulation of the water, [in Russian]. Probl of the Arctic and Antarc 65:75-97.

Scully MP (1975) Computation of helicopter rotor wake geometry and its influence on rotor harmonic airloads. Massachusetts Inst. of Technology, Publ. ARSL TR 152–1, Cambridge.

Siedler G, Church J, Gould J 2001 (Ed.) Ocean circulation and climate: observing and modelling the global ocean. International Geophysics Series, Academic Press: San Diego. 77, ISBN 0-12-641351-7. XIX, p 715.

Søiland H, Rossby T (2013). On the structure of the Lofoten Basin Eddy. Journal of Geophysical Research: Oceans, 118(9): 4201-4212.

Søiland H, Chafik L, Rossby T (2016). On the long-term stability of the Lofoten Basin Eddy. Journal of Geophysical Research: Oceans, 121(7): 4438-4449.

Vaillancourt RD, Marra J, Seki MP, Parsons ML, Bidigare RR (2003) Impact of a cyclonic eddy on phytoplankton community structure and photosynthetic competency in the subtropical North Pacific Ocean. Deep Sea Res:I 50:829-847.

Volkov DL, Belonenko TV, Foux VR (2013) Puzzling over the dynamics of the Lofoten Basin – a sub-Arctic hot spot of ocean variability. Geophys Res Lett 40(4):738–743. doi:10.1002/grl.50126.

Volkov DL, Kubryakov AA, Lumpkin R (2015) Formation and variability of the Lofoten basin vortex in a high-resolution ocean model. Deep Sea Res:I 105:142-157. doi:10.1016/j.dsr.2015.09.001.

Volkov DL, Lee T, Fu LL (2008) Eddy-induced meridional heat transport in the ocean. Geoph Res Lett 35(20).

Walsh D, Richardson PL, Lynch J (1997). Observations of tilting meddies. Oceanographic Literature Review, 2(44), 84.

White M, Bashmachnikov I, Aristegui J, Martins A (2007) Physical Processes and Seamount Productivity. In: Seamounts: Ecology, Conservation and Management (eds. Pitcher TJ, Morato T, Hart PJB, Clark MR, Haggan N, Santos RS). Fish and Aquatic Resources Series, Blackwell, Oxford, UK, Chapter 4, pp. 65-84.

Wunsch C, Ferrari R (2004) Vertical mixing, energy, and the general circulation of the oceans. Annual Reviews of Fluid Mech 36:281-314.

Yu LS, Bosse A, Fer I, Orvik KA, Bruvik EM, Hessevik I, Kvalsund K (2017). The Lofoten Basin eddy: Three years of evolution as observed by Seagliders. J Geophys Res. Oceans 122: 6814–6834, doi:10.1002/2017JC012982..

Zhmur VV (2011) Mesoscale vortices of the ocean, [in Russian], Moscow, GEOS, 384 p.